J Fluoresc (2014) 24:1447–1455
DOI 10.1007/s10895-014-1428-6

ORIGINAL PAPER

Spectroscopic Studies on Photoelectron Transfer from 2-(furan-2-yl)-1-phenyl-1H-phenanthro[9,10-d]imidazole to ZnO, Cu—doped ZnO and Ag—doped ZnO

V. Thanikachalam · A. Arunpandiyan · J. Jayabharathi · C. Karunakaran · P. Ramanathan

Received: 21 April 2014 / Accepted: 7 July 2014 / Published online: 9 August 2014

Abstract The 2-(furan-2-yl)-1-phenyl-1H-phenanthro[9,10-d]imidazole [FPI] has been designed and synthesized as fluorescent sensor for nanoparticulate ZnO. The present work investigates the photoelectron transfer (PET) from FPI to ZnO, Cu-doped ZnO and Ag- doped ZnO nanoparticles using electronic and life time spectral measurements. Broad absorption along with red shift indicates the formation of charge-transfer complex [FPI−Nanoparticles]. The photophysical studies indicate lowering of HOMO and LUMO energy levels of FPI on adsorption on ZnO due to FPI− ZnO interaction. The obtained binding constant implies that the binding of FPI with nanoparticles was influenced by the surface modification of ZnO nanoparticles with Cu and Ag.

Keywords Life time · PET · ZnO, FPI− ZnO · Cu-doped ZnO · Ag- doped ZnO

Introduction

Nanoparticles exhibit potential applications in biological fields like clinical diagnostic assays, drug delivery systems and cellular imaging [1–3]. Nanoparticles can be used as drug carriers because they possess enormous surface area and due to their submicron size they can efficiently be taken up by the cells [4]. ZnO is an attractive semiconductor material with wide direct band gap (3.37 eV), large exciton binding energy (60 meV) and a hexagonal structure and have significant applications in optoelectronics, sensors and actuators [5, 6]. Additionally, ZnO is also a biocompatible material with a high isoelectric point (IEP) of about 9.5, which make it suitable for absorption of low IEP proteins such as glucose oxidase, as the protein immobilization is primarily driven by electrostatic interaction [7]. Hence, ZnO is one of the most desirable platforms for binding enzyme and a promising material for a wide range of biosensor applications.

Au, Ag, or Pt noble metal coated ZnO is important for photoelectron transfer (PET) in the bulk and interface of ZnO semiconductors [8]. Under illumination of UV light, the exciton absorption bands of ZnO are strongly bleached due to the accumulation of conduction band electrons [9]. Thus, the efficiency of both the photocatalysis and photoelectric energy conversion can be greatly enhanced by depositing noble metals on the surface of ZnO [10]. The properties and applications of noble metal ZnO nanostructured materials are also determined by its morphology, structure and the organization of nanostructured ZnO architectures [11–14]. ZnO based various ceramics were synthesised by liquid phase sintering of ZnO powder of different sizes and morphologies. The highest occupied molecular orbital (HOMO) and lowest unoccupied molecular orbital (LUMO) potentials for the designed sensor must match with the conduction and valence band edges of the semiconductor nanocrystals [15–23]. In this paper we report the binding of 2-(furan-2-yl)-1-phenyl-1H-phenanthro[9,10-d]imidazole with ZnO, Cu-doped ZnO and Ag- doped ZnO nanoparticles was probed through absorption, fluorescence, cyclic voltammetry and life time spectral measurements. Electron injection from the excited FPI into the conduction band of nanoparticles was detected.

Experimental

Materials

Phenanthrene-9,10-dione, aniline, furfuraldehyde and all other reagents have been purchased from S.D. fine chemicals.

V. Thanikachalam · A. Arunpandiyan · J. Jayabharathi (✉) · C. Karunakaran · P. Ramanathan
Department of Chemistry, Annamalai University, Annamalainagar 608 002, Tamilnadu, India
e-mail: jtchalam2005@yahoo.co.in

Synthesis of 2-(furan-2-yl)-1-phenyl-1H-phenanthro[9,10-d] imidazole [FPI] by InF_3

A mixture of furfuraldehyde (1 mmol), phenanthroquinone (1 mmol), aniline (1 mmol), ammonium acetate (1 mmol) and indium trifluoride (InF_3) (1 mol %) was stirred at 80 °C. The progress of the reaction was monitored by TLC (Scheme 1). After completion of the reaction, the mixture was cooled, dissolved in acetone and filtered. The product was purified by column chromatography using benzene: ethyl acetate (9:1) as the eluent. M.p. 228ºC, Anal. calcd. for $C_{25}H_{16}N_2O$: C, 83.31; H, 4.47; N, 7.77; O, 4.44. Found: C, 83.29; H, 4.49; N, 7.76; O, 4.43. ^{1}H NMR (400 MHz, DMSO): δ 6.87 (s, 1H), 7.54 (s, 1H), 8.12 (s, 1H),7.35 (d, 1H), 7.82–7.77 (m, 7H), 8.29 (d, *J*=6.8Hz, 1H), 8.46 (d, *J*=7.2Hz, 1H), 8.97–8.85 (m, 3H). ^{13}C NMR (100 MHz, DMSO):δ 110.86, 111.68, 112.80, 114.10, 120.43, 121.98, 122.23, 124.08, 124.26, 125.06, 125.87, 126.71, 127.05, 127.95, 128.29, 128.51, 128.70, 130.64, 134.38, 137.72, 141.79, 143.54, 144.33, 146.59, 154.18. MS: m/z. 360 [M+].

Synthesis of Nanocrystalline Oxides by Sol–Gel Method

To zinc acetate (0.1 g) solution (with or without $Cu(NO_3)_2$/$Ag(NO_3)_2$) under continuous stirring, aqueous ammonia (1:1) was added drop wise to reach a pH of 7 and the stirring was continued for another 30 min. The formed glassy like white gel was allowed to age overnight. It was filtered, washed with water and ethanol, dried at 100 °C for 12 h calcinated at 500 °C for 2 h (heating rate 10 °C min $^{-1}$) to pale grey solid.

Spectral Measurements

The ultraviolet–visible (UV–vis) spectra were obtained with Perkin Elmer Lambda 35 UV–vis spectrophotometer and corrected for background absorption due to solvent. Photoluminescence (PL) spectra were recorded on a PerkinElmer LS55 fluorescence spectrometer. NMR spectra were recorded on Bruker 400 MHz NMR spectrometer. The mass spectra of the samples were obtained using an Agilent LCMS VL SD in electron ionization mode. Cyclic voltammetry (CV) analyses were performed by using CHI 630A potentiostat electrochemical analyzer. Fluorescence lifetime measurements were carried out with a nanosecond time correlated single photon counting (TCSPC) spectrometer Horiba Fluorocube-01-NL lifetime system with Nano LED (pulsed diode exCitation source) as the excitation source and TBX-PS as detector. The absolute PL quantum yields were measured by comparing fluorescence intensities (integrated areas) of a standard sample (coumarin 46). Theoretical calculations were performed using density functional theory (DFT) as implemented with Gaussian-03 program using the Becke3-Lee-Yang-Parr (B3LYP) functional supplemented with the standard 6-31G (d, p) basis set [24].

Methanolic solution of the FPI of required concentration was mixed with the nanoparticles dispersed in methanol at different loading and the absorption (1×10^{-5} M) and emission (1×10^{-8} M) spectra were recorded. The ZnO, Cu- ZnO and Ag- ZnO nanoparticles were dispersed under sonication in methanol.

Results and Discussion

Scanning Electron Micrograph (SEM) and Energy Dispersive Spectrum (EDS)

The scanning electron micrographs of the synthesized nanoparticles are displayed in Fig. 1. The SEM images show the agglomeration of the synthesized nanoparticles. The Ag^+ ion is larger (radius 1.22 A°) than that of Zn^{2+} (0.72 A°) and cannot be incorporated in to the ZnO lattice. Hence silver preferentially choose to segregate around the ZnO grain boundaries. Energy Dispersive X-ray (EDX) spectra of ZnO and Cu doped ZnO are shown as Fig. 2. It confirms the presence of dopant in the doped oxides.

Ground State Interaction Between FPI–ZnO Nanoparticle

The absorption spectra of FPI show a superposition of the bands corresponding to the donor and acceptor subunits which seem to be only slightly perturbed by their interactions. The three absorption bands at 210, 255 and 359 nm are assigned to $^1(\pi–\pi^*)$ transition correspond in Platt's notation to ^1L_b, ^1L_a and ^1B_a excited states. The low and high energy transitions, $^1L_b \leftarrow S_0$, $^1L_a \leftarrow S_0$ and $^1B_a \leftarrow S_0$, respectively are observed in the absorption spectra [25, 26]. The low energy absorption region of the FPI containing furfuryl as an electron acceptor indicates the presence of additional charge transfer singlet states.

When Cu-doped ZnO nanoparticles were added to FPI solution, the absorption band around 210 nm enhances along with red shift and no significant shift was observed with the absorption around 255 and 359 nm at higher concentration of Cu-doped ZnO. These changes in absorption of FPI imply a strong electronic coupling between FPI and Cu-doped ZnO nanoparticles. As a result there may be changes in electronic distribution in FPI which causes an increase in molar absorbance along with bathochromic shift due to the complex formation of FPI − Cu-doped ZnO. The absorption characteristics of FPI with ZnO have been shown in Fig. 3. The absorption of FPI at 210 nm was shifted to 240 nm by ZnO. However, the shift is around 285 and 280 nm, respectively, with the same concentration of Cu-doped ZnO and Ag- doped

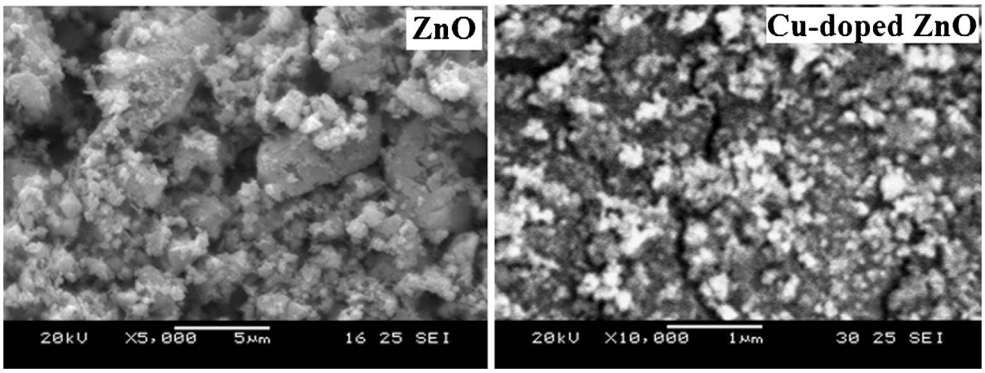

Fig. 1 SEM image of ZnO and Cu-ZnO

ZnO nanoparticles. No significant shift was detected for the absorption at longer wavelengths. The binding strength of FPI with nanoparticles were calculated using Benesi- Hildebrand equation [27–29], $\frac{1}{\Delta A} = \frac{1}{A_C - A_0} + \frac{1}{K(A_C - A_0)[\text{nanoprticels}]}$, where ΔA is the change in absorbance at a fixed wavelength, A_0 and A_c are the absorbance of free sensitizer and the complex [FPI-Nanoparticles], respectively For the complex formation a linear relationship will be obtained between $1/\Delta A$ and 1/[Nanoparticles]. From the ratio of the intercept $1/(A_c - A_0)$ to the slope $1/K\ (A_c - A_0)$, the binding constant (K) have been calculated and are given in Table 1. The higher K value in the presence of Cu modified ZnO nanoparticles indicates the strong binding of FPI with Cu-doped ZnO. Hence the presence of Cu metal with ZnO nanoparticles results in efficient electronic coupling with FPI.

Fluorescence Enhancement

The emission spectra of FPI in presence of ZnO and doped ZnO nanoparticles (Cu- doped ZnO and Ag- doped ZnO)

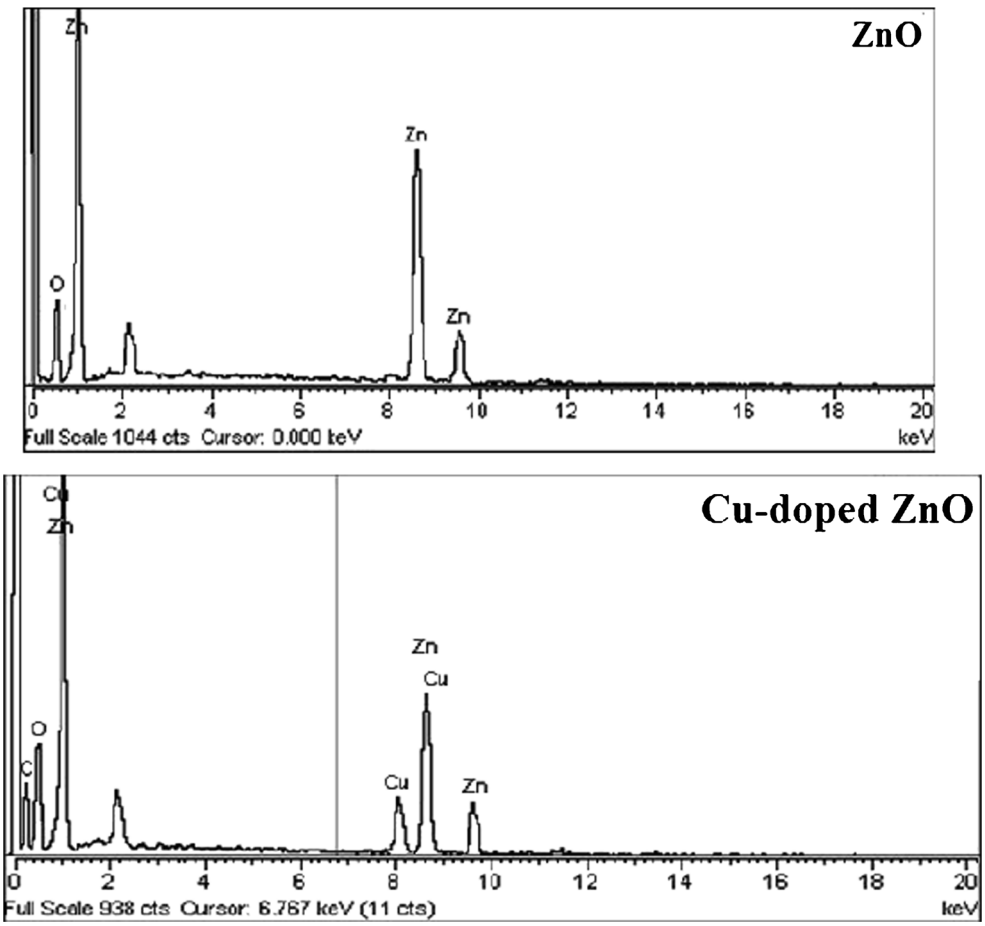

Fig. 2 EDX spectra of ZnO and Cu-ZnO

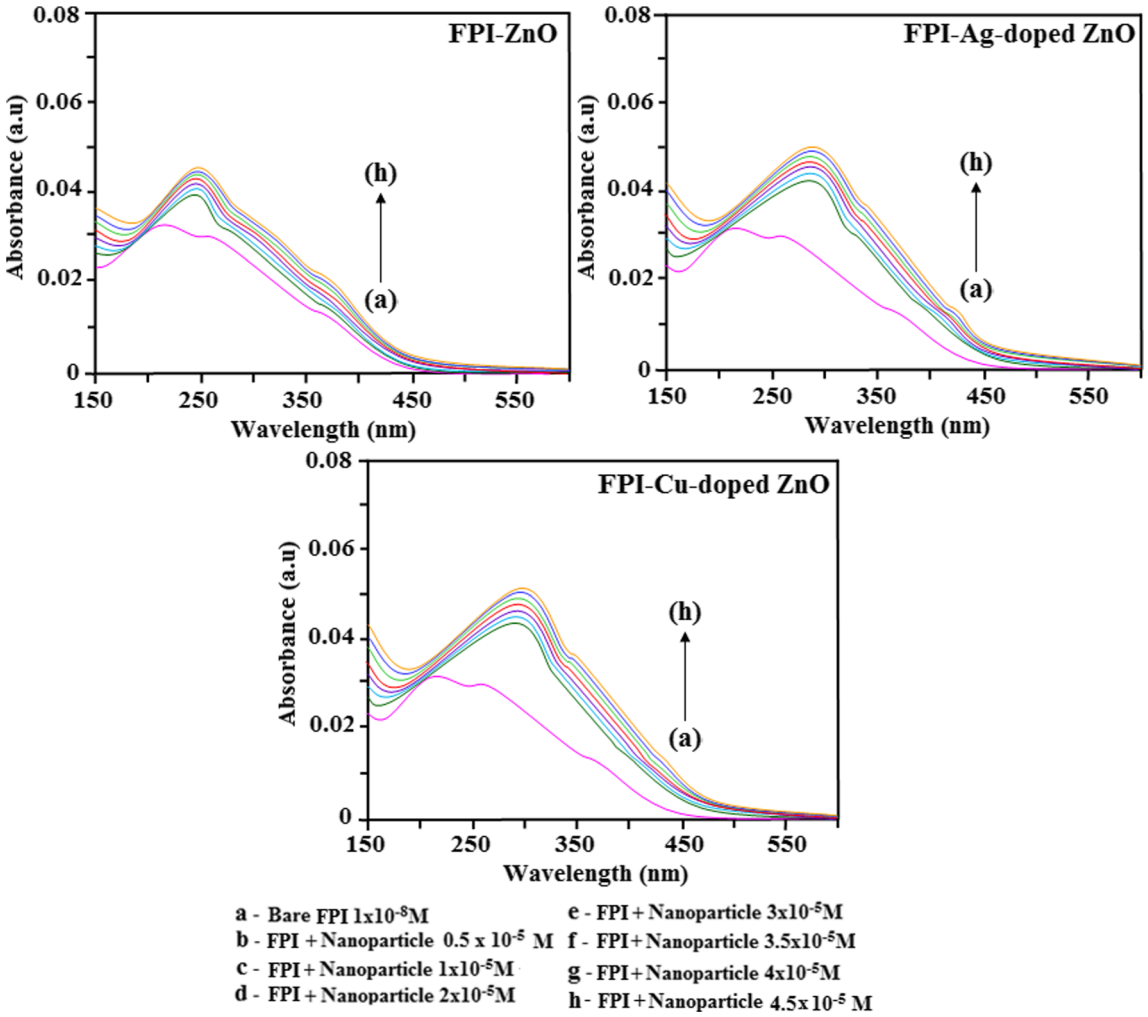

Fig. 3 Absorption spectra of FPI in presence and absence of ZnO, Cu-ZnO and Ag-ZnO nanoparticles

dispersed at different loading and also in their absence are displayed in Fig. 4. The nanoparticle enhances the emission of FPI remarkably without shifting its emission maximum at 405 nm. This indicates that the nanocrystal do not modify the excitation process of the ligand. The enhanced emission at 405 nm observed with the dispersed semiconductor nanoparticle is due to the adsorption of FPI on semiconductor surface. This is because of effective electron transfer from the excited state of FPI to the conduction band (CB) of the semiconductor nanoparticle. Fluorescence enhancement arises due to the formation of complex [FPI–Nanoparticles]. The linear variation of I/I_0 versus [Nanoparticles] is shown in Fig. 4. The determined slope value of unity shows that each molecule is bound to one ZnO and the calculated binding constant (K) is in good agreement with those calculated from absorption measurements. The order of binding constant (*K*) is Cu-doped ZnO > ZnO > Ag- doped ZnO. The formation constant of FPI– nanoparticles is in agreement with the binding

Table 1 Lifetime (τ, ns), radiative rate constant (k_r, 10^8 s^{-1}), nonradiative rate constant (k_{nr}, 10^8 s^{-1}), electron transfer rate constant (k_{et}, 10^7 s^{-1}), binding constant (K, M), binding sites (n) and evaluation of overlap integral (J, $\times 10^{-12}$ cm^{-3}/mol), energy transfer efficiency E, maximal critical distance (R_0, $\times 10^{-9}$ m) and acceptor and donor distance (r_0, nm)

Complex	τ	k_r	k_{nr}	k_{et}	J	E	R_0	r_0	K	*n*
FPI	3.72	0.80	1.9	–	–	–	–	–	–	–
FPI ….ZnO	3.33	0.90	2.1	3.0	5.01	0.28	0.79	0.95	2.98×10^8	0.97
FPI ….Ag-ZnO	3.42	0.79	2.2	2.2	6.25	0.19	0.85	1.23	9.02×10^7	0.91
FPI ….Cu-ZnO	3.21	0.69	2.6	4.2	4.83	0.31	0.82	0.91	9.89×10^9	0.98

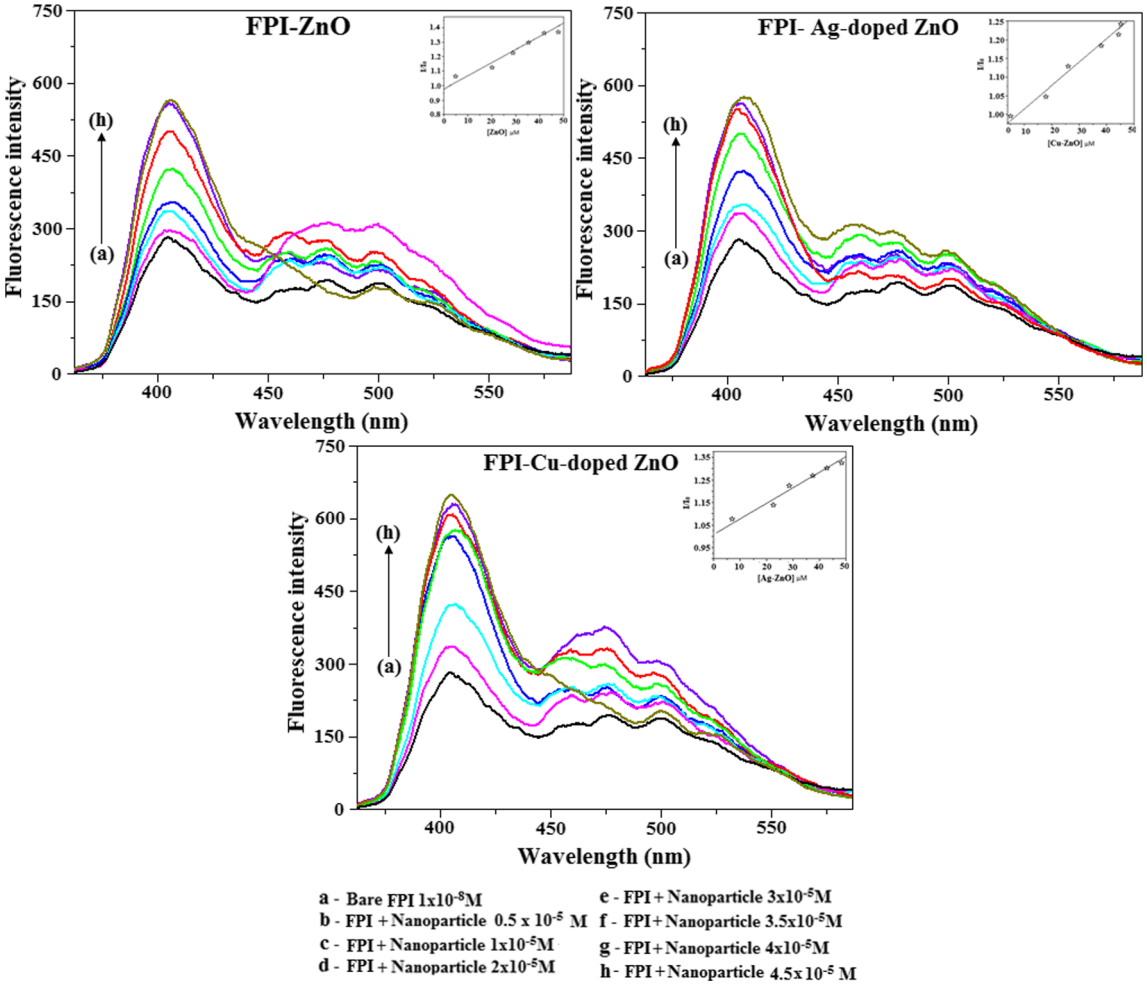

Fig. 4 **a** Fluorescence enhancement of benzimidazole derivative in the presence and absence of various concentrations of ZnO nanoparticle; **b** Inhibition of fluorescence enhancement of benzimidazole derivative on doping ZnO with Cu; **c** Inhibition of fluorescence enhancement of benzimidazole derivative on doping ZnO with Ag

tendency of the metal ion/metal in the nanoparticles with FPI. In copper doped zinc oxide, Cu^{2+} tends to bind with function (Fig. 5). In Ag- doped ZnO, silver is in metallic state; the binding of the noble metal silver with FPI is likely to be the weakest of the three. That is, the binding of Cu^{2+} in the nanoparticle is strong. On the other hand, the presence of metallic silver on ZnO surface weakens the binding. This is because in Ag- doped ZnO, Ag^0 is deposited on the surface of the crystal there by inhibiting the binding of the ligand with ZnO. In Cu- doped ZnO, copper is likely to be present in the cationic sites or the interstitial positions thereby not inhibiting the binding of ligand with ZnO. Furthermore the doped Cu^{2+} on the surface of ZnO may bind with the ligand. Both the dopants suppress the enhancement of fluorescence and the suppression is more by copper than by silver doping. The possible reason is Cu^{2+} in Cu- doped ZnO may bind with the ligand and this binding could be much stronger than that by Zn^{2+}. The binding of Ag with ligand is not as strong as that of Cu^{2+}.

Electrochemical Measurements

Cyclic voltametric studies were carried out to probe the efficient binding of ZnO, Cu- doped ZnO and Ag- doped ZnO nanoparticles with FPI. Figure 5 shows the cyclic voltammogram (CV) of FPI and FPI with ZnO, Cu- doped ZnO and Ag-doped ZnO nanoparticles. In the presence of ZnO, Cu- doped ZnO and Ag- doped ZnO nanoparticles the CV of FPI shows a shift in peak potentials along with decrease in peak current [30]. It is evident that the ZnO, Cu- doped ZnO and Ag- doped ZnO nanoparticles have efficient binding with FPI which supports the electronic spectral results.

Enhancement Mechanism

From the onset oxidation potential (E_{ox}) and the onset reduction potential (E_{red}) of the FPI derivative, HOMO and LUMO energy levels have been calculated according to the following equations [31], $HOMO = -e(E_{ox} + 4.71)$

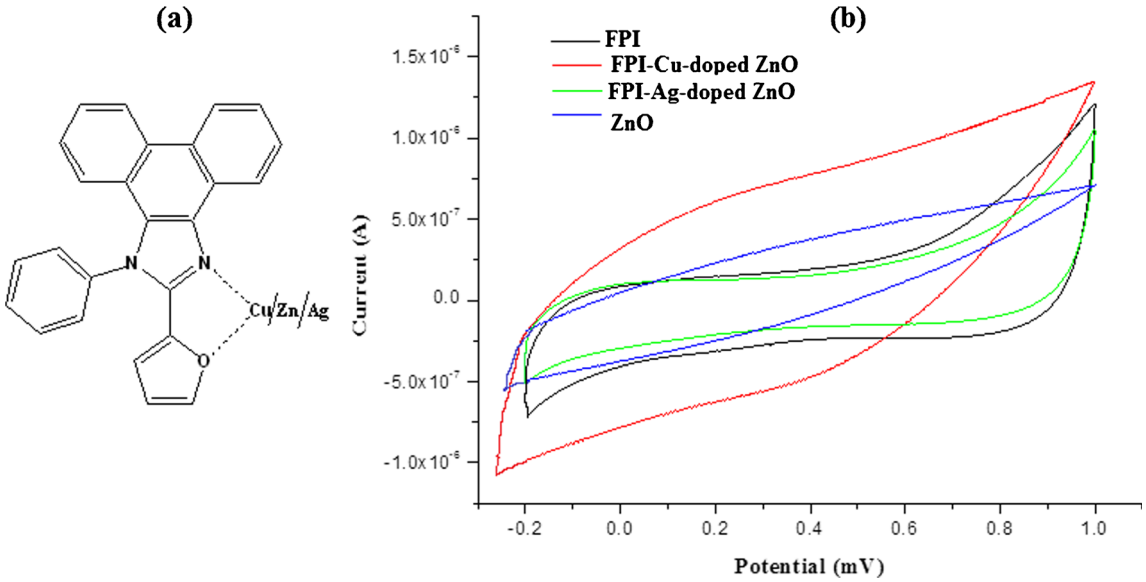

Fig. 5 **a** Schematic representation for complex formation; **b** Cyclic voltammogram of (1) FPI (1×10^{-5} M), and (2) FPI (1×10^{-5} M) in presence of ZnO nanoparticles (1×10^{-5} M)

(eV); LUMO=$-e(E_{red}+4.71)$ (eV). On the basis of the HOMO and LUMO energy levels of FPI and CB energy levels of ZnO, Cu- doped ZnO and Ag- doped ZnO (Fig. 6a), the electron injection is thermodynamically allowed from the excited singlet of the FPI to the CB of ZnO/Cu- doped ZnO and Ag- doped ZnO. Figure 6b presents the HOMO and LUMO energy levels of an isolated molecule along with the CB and valence band (VB) edges of ZnO nanoparticles. On adsorption of FPI on ZnO surface, the HOMO and LUMO may interact with CB and VB of ZnO and as a consequence the energy levels of HOMO and LUMO may be lowered. The modified HOMO and LUMO energy levels presented in Fig. 6c suggests enhancement of fluorescence of FPI by ZnO nanocrystal. On illumination at 245 nm

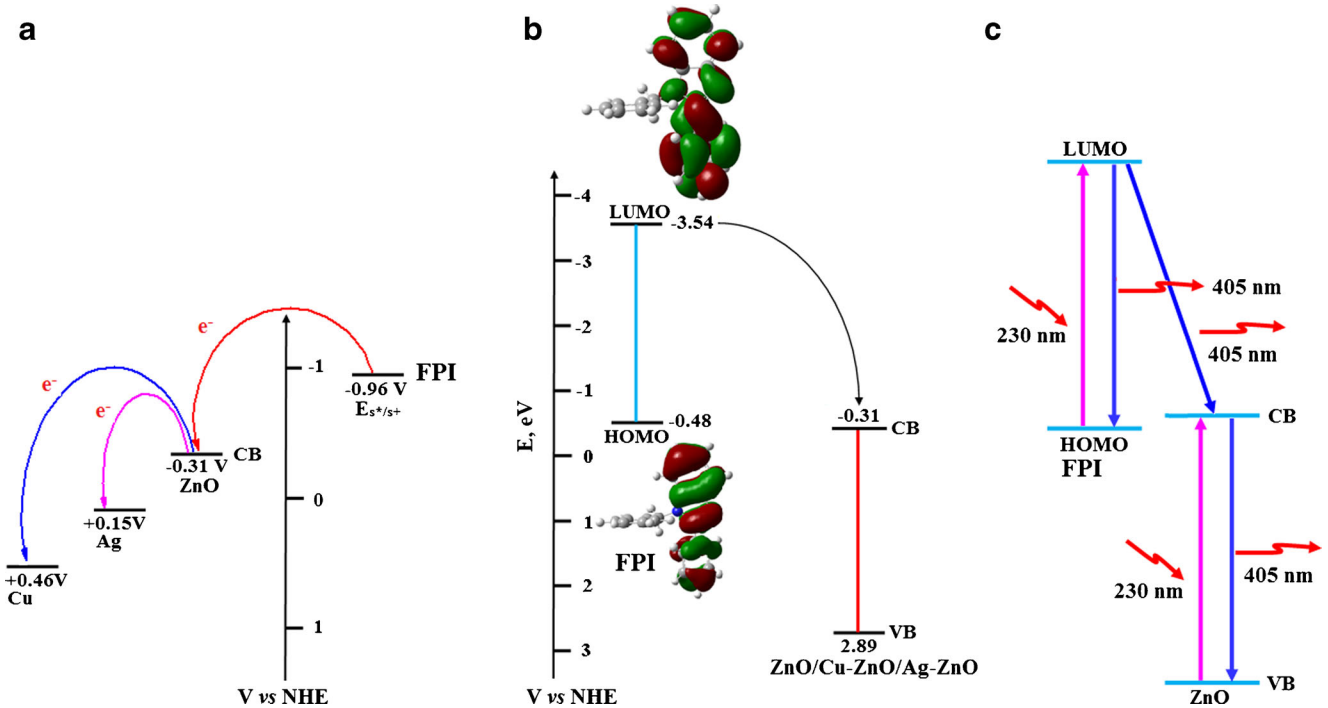

Fig. 6 **a** Energy level diagram; **b** HOMO and LUMO energy levels of an isolated molecule along with the conduction band and valence band edges of ZnO nanoparticle; **c** Enhancement of fluorescence of derivative by ZnO nanocrystals

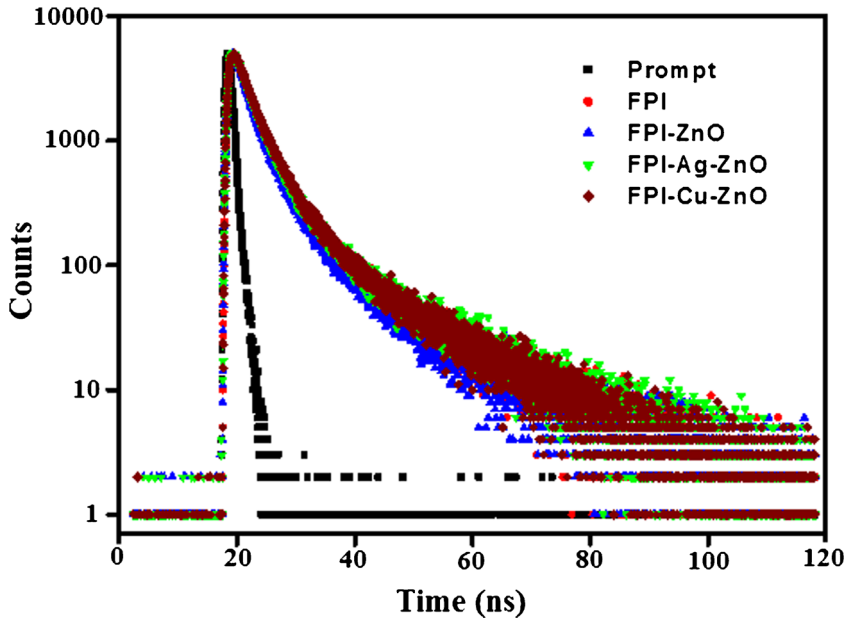

Fig. 7 Fluorescence lifetime spectra of FPI and complex FPI-ZnO, FPI-Ag-ZnO and FPI-Cu-ZnO nanoparticles

both the ligand and nano semiconductor are excited. Duel emission is expected due to LUMO→HOMO and CB→VB electron transfer. ZnO exhibits emission at ~420 nm because of band edge free excitons [28, 29] and the excited FPI emits fluorescence at 405 nm Also possible is electron jump from the excited ligand to the nanocrystals. The electron in the LUMO of the excited ligand is of higher energy compared to that of the CB of ZnO nanocrystals. The emission intensity of FPI bound to ZnO is far larger than that of the isolated molecule. With the FPI adsorbed on ZnO the semiconductor is also excited on irradiation. The recombination of the electron in the CB or singly or doubly occupied oxygen vacancies with the hole in the VB results in emission at 405 nm. In addition, emission from the LUMO of the FPI adsorbed on ZnO to the CB of ZnO at 405 nm is possible. Due to the additional path opened up for emission the emission intensity is increased. On interaction of FPI with ZnO the polar ZnO surface enhances the delocalisation of the π electrons and lowers the HOMO and LUMO energy levels of the adsorbed FPI due to ligand—semiconductor complex formation [32]. If the HOMO and LUMO energy levels of FPI lowered by about 0.17 eV on complexation with ZnO the energy difference between LUMO and CB of ZnO will be about 3.06 eV. This corresponds to emission at 405 nm. The addition path opened due to LUMO→CB electron jump increase the intensity of emission at 405 nm. The chemical affinity between the nitrogen atom of the ligand and zinc ion on the surface of the nano oxide may be a reason for strong interaction of the ligand on nanoparticle causes the enhancement.

Free-Energy Change (ΔG_{et}) for Electron Transfer Process

The thermodynamic feasibility of excited state electron transfer reaction has been confirmed by the calculation of free energy change by employing the well known Rehm-Weller expression [32], $\Delta G_{et}=E^{1/2}{}_{(ox)}-E^{1/2}{}_{(red)}-E_s+C$, where, $E^{1/2}{}_{(ox)}$ is the oxidation potential of FPI, $E^{1/2}{}_{(red)}$ is the reduction potential of ZnO nanoparticle, i.e., the CB potential of nanoparticle, Es is the excited state energy of derivative and C is the coulombic term. Since the ligand is neutral and the

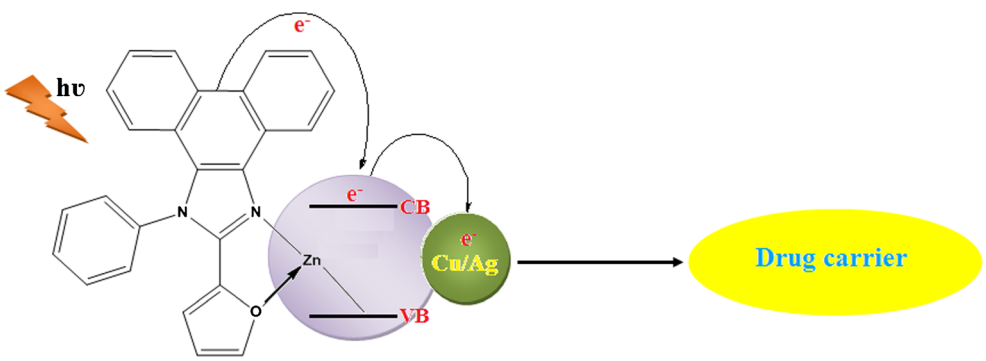

Fig. 8 Mechanism of electron transfer

solvent used is polar in nature, the coulombic term in the above expression can be neglected [33]. The values of ΔG_{et} is calculated as −3.66 eV. The high negative values indicate the thermodynamic feasibility of the electron transfer process [34].

Fluorescence Lifetime Measurements

An alternative way to rationalize the behaviour observed in the present study is by considering the fluorescence lifetime of FPI concentration. Figure 7 displays the fluorescence decay of FPI along with FBI-ZnO, FBI- Cu – doped ZnO and FBI- Ag-doped ZnO. The decay follows a bi-exponential fit indicating FPI is in two excited states - one is likely to be the configuration in which the furfuryl moiety is coplanar with the imidazole ring and other is one with the furfuryl ring is perpendicular to the imidazole ring. Theoretical calculations show the perpendicular configuration as most stable and hence the observed longer lifetime is attributed to the same. The radiative and non-radiative decay of the excited state have been obtained using the quantum yields and lifetimes. The formula employed to calculate the radiative (k_r) and non-radiative (k_{nr}) rate constants is $k_r=\Phi_p/\tau$; $k_{nr}=(1/\tau)-(\Phi_p/\tau)$; $\tau=(k_r+k_{nr})^{-1}$, where k_r and k_{nr} are the radiative and non-radiative deactivation, τ is the lifetime. The k_r and k_{nr} values are displayed in Table 1. The decrease in lifetime for the complex formation FPI-Nanoparticles was correlated with electron process. The rate constants for electron transfer process (k_{et}) from excited state of FPI to semiconductor nanoparticles can be calculated using the equation, $k_{et}=1/\tau_{ads}-1/\tau$ and the calculated k_{et} values are shown in Table 1.

According to Forster's energy transfer theory, the energy transfer efficiency is related not only to the distance between the acceptor and donor (r_0), but also to the critical energy transfer distance (R_0). That is, $E = R^6_0/(R^6_0 + r^6_0)$, where, R_0 is the critical distance when the transfer efficiency is 50 % and $R^6_0=8.8\times10^{-25}K^2N^{-4}\,\varphi\,J$, where, K^2 is the spatial orientation factor of the dipole, N is the refractive index of the medium, φ is the fluorescence quantum yield of the donor and J is the overlap integral of the fluorescence emission spectrum of the donor and the absorption spectrum of the acceptor. The value of J can be calculated by using the equation $J = \int F(\lambda)\varepsilon(\lambda)\lambda^4 d\lambda / F(\lambda)d\lambda$, where, $F(\lambda)$ is the fluorescence intensity of the donor and $\varepsilon(\lambda)$ is molar absorptivity of the acceptor. The evaluated parameters J, E, R_0 and r_0 are listed in Table 1. Obviously, the calculated value of R_0 is in the range of maximal critical distance. This is in accordance with the conditions of Forster's energy transfer theory [35] and suggests that energy transfer occurs between the semiconductor nanoparticles and FPI with high probability. The evaluated distance between the FPI and the ZnO, Cu- doped ZnO and Ag- doped ZnO are the same and this supports the ZnO-FPI binding in all the cases. Similar trend is observed with energy transfer efficiency; the E values of ZnO, Cu- doped ZnO and Ag- doped ZnO nanoparticles are 0.28, 0.19 and 0.31, respectively. All these results put forward that the optoelectronic behavior of FPI with ZnO will be enhanced in the presence of Cu and Ag metal which implies its potential application in the field of nano-drug carriers (Fig. 8). The electron injected from LUMO of FPI to CB of Ag or Cu- doped ZnO which will react with oxygen molecules to produce superoxide radicals which damages DNA in photodynamic therapy or it can be utilized for solar cell applications [36, 37]. This implies its potential application in the field of photodynamic therapy, solar cells etc., The ligand bond to the nanoparticle may reach the required site for possible application as photodynamic therapy. To put in detail the organic molecule attached to the semiconductor nanoparticle could reach the diseased cell and bound to it. Thus the nanosemiconductor is linked to the attached cell enabling photodynamic therapy.

Conclusion

Photoinduced interactions of FPI with nanoparticles were investigated using various spectroscopic measurements. Binding constant values obtained from the absorption and fluorescence measurements demonstrated that the binding of ZnO nanoparticles with FPI greatly influenced by the surface modification with Cu and Ag. Electron from the excited FPI transferred to the conduction band of ZnO and quickly migrated to the Cu^{2+} or Ag^0. All these results put forward that the optoelectronic behavior of FPI with ZnO is influenced by the presence of Cu^{2+} and Ag^0 which implies its potential application in the field of nano-drug carriers.

Acknowledgments One of the authors Prof. J. Jayabharathi is thankful to DST [No. SR/S1/IC-73/2010], DRDO (NRB-213/MAT/10-11), UGC (F. No. 36-21/2008 (SR)) and CSIR (NO 3732/NS-EMRII) for providing funds to this research study.

References

1. Bruchez M, Moronne M, Gin P, Weiss S, Alivisatos AP (1998) Semiconductor nanocrystals as fluorescent biological labels. Science 281:2013–2016
2. Wu X, Liu H, Liu J, Haley K, Treadway J, Larson J, Ge N, Peals F, Bruchez M (2003) Immunofluorescent labeling of cancer marker Her2 and other cellular targets with semiconductor quantum dots. Nat Biotechnol 21:41–46
3. Gao X, Cui Y, Levenson RM, Chung L, Nie S (2004) In vivo cancer targeting and imaging with semiconductor quantum dots. Nat Biotechnol 22:969–976
4. Wiseman A (1985) Handbook of enzyme biotechnology. Horwoodi, Chichester
5. Masuda Y, Kato K (2008) High c-axis oriented stand-alone ZnO self-assembled film. Cryst Growth Des 8:275–279

6. Zhang XM, Lu MY, Zhang Y, Chen LJ, Wang ZL (2009) Fabrication of a high-brightness blue-light-emitting diode using a ZnO-nanowire array grown on p-GaN thin film. Adv Mater 21:2767–2770
7. Topoglidis E, Cass AEG, Regan BO, Durrant JR (2001) Immobilisation and bioelectrochemistry of proteins on nanoporous TiO_2 and ZnO films. J Electroanal Chem 517:20–27
8. Subramanian V, Wolf EE, Kamat PV (2003) Green emission to probe photoinduced charging events in ZnO-Au nanoparticles. charge distribution and fermi-level equilibration. J Phys Chem B 107:7479–7485
9. Chen S, Ingram RS, Hostetler MJ, Pietron JJ, Murray RW, Schaaff TG, Khoury JT, Alvarez MM, Whetten RL (1998) Gold nanoelectrodes of varied size: transition to molecule-like charging. Science 280:2098–2101
10. Ozgur U, Alivov I, Liu C, Teke A, Reshchikov MA, Doan S, Avrutin V, Cho SJ, Morkoc H (2005) A comprehensive review of ZnO materials and devices. J Appl Phys 98:041301
11. Huang MH, Mao S, Feick H, Yan HQ, Wu YY, Kind H, Weber E, Russo R, Yang PD (2001) Room-temperature ultraviolet nanowire nanolasers. Science 292:1897–1899
12. Wang YW, Zhang LD, Wang GZ, Peng XS, Chu ZQ, Liang CH (2002) Catalytic growth of semiconducting zinc oxide nanowires and their photoluminescence properties. J Cryst Growth 234:171–175
13. Feng X, Feng L, Jin M, Zhai J, Jiang L, Zhu D (2004) Reversible super-hydrophobicity to super-hydrophilicity transition of aligned ZnO nanorods films. J Am Chem Soc 126:62–63
14. Law M, Greene LE, Jhonson JC, Saykally R, Yang P (2005) Nanowire dye-sensitized solar cells. Nat Mater 4:455–459
15. Jayabharathi J, Thanikachalam V, Kalaiarasi V, Jayamoorthy K (2014) Characterization and electronic spectral studies of 2-(naphthalen-1-yl)-4,5-diphenyl-1H-imidazole bound Fe_2O_3 nanoparticles. Spectrochim Acta A 120:84–87
16. Jayabharathi J, Thanikachalam V, Kalaiarasi V, Jayamoorthy K (2014) Enhancing photoluminescent behavior of 2-(naphthalen-1-yl)-1,4,5-triphenyl-1H-imidazole by ZnO and Bi_2O_3. Spectrochim Acta A 118: 182–186
17. Karunakaran C, Jayabharathi J, Sathishkumar R, Jayamoorthy K (2013) Photoinduced electron transfer from Phenanthroimidazole to nano WO_3, CuO and ZrO_2. A new approach on LUMO - CB energy binding efficiency relationship. Measurement 46:3261–3267
18. Karunakaran C, Jayabharathi J, Jayamoorthy K (2013) Fluorescence enhancing and quenching of TiO2 by benzimidazole. Sensors Actuators B 188:207–211
19. Karunakaran C, Jayabharathi J, Jayamoorthy K (2013) Photoinduced electron transfer from benzimidazole to nano WO_3, CuO and Fe_2O_3. A new approach on LUMO—CB energy-binding efficiency relationship. Sensors Actuators B 182:514–520
20. Karunakaran C, Jayabharathi J, Sathishkumar R, Jayamoorthy K, Vimal K (2013) Contrasting emission behaviour of phenanthroimidazole with rutile and anatase TiO_2 nanoparticles. J Lumin 138:235–241
21. Karunakaran C, Jayabharathi J, Jayamoorthy K, Brindha Devi K (2012) Photosensitization of imidazole derivative by ZnO nanoparticle. J Fluoresc 22:1047–1053
22. Karunakaran C, Anilkumar P, Gomathisankar P (2011) Photoproduction of iodine with nanoparticulate semiconductors and insulators. Chem Cent J 123: 5:31
23. Karunakaran C, Rajeswari V, Gomathisankar P (2011) Enhanced photocatalytic and antibacterial activities of sol–gel synthesized ZnO and Ag-ZnO. Mater Sci Semicond Process 14:133–138
24. Frisch MJ, Trucks GW, Schlegel HB, Scuseria GE, Robb MA, Cheeseman JR, Montgomery JA Jr., Vreven T, Kudin KN, Burant JC, Millam JM, Iyengar SS, Tomasi J, Barone V, Mennucci B, Cossi M, Scalmani G, Rega N, Petersson GA, Nakatsuji H, Hada M, Ehara M, Toyota K, Fukuda R, Hasegawa J, Ishida M, Nakajima T, Honda Y, Kitao O, Nakai H, Klene M, Li X, Knox JE, Hratchian HP, Cross JB, Adamo C, Jaramillo J, Gomperts R, Stratmann RE, Yazyev O, Austin AJ, Cammi R, Pomelli C, Ochterski JW, Ayala PY, Morokuma K, Voth GA, Salvador P, Dannenberg JJ, Zakrzewski VG, Dapprich S, Daniels AD, Strain MC, Farkas O, Malick DK, Rabuck AD, Raghavachari K, Foresman JB, Ortiz JV, Cui Q, Baboul AG, Clifford S, Cioslowski J, Stefanov BB, LiuG, Liashenko A, Piskorz P, Komaromi I, Martin RL, FoxDJ, Keith T, Al-Laham MA, Peng CY, Nanayakkara A, Challacombe M, Gill PMW, Johnson B, Chen W, Wong MW, Gonzalez C, Pople JA (2003) Gaussian Inc, Pittsburgh
25. Czerwieniec R, Herbich J, Kapturkiewicz A, Nowacki J (2000) Radiative electron transfer in planar donor–acceptor quinoxaline derivatives. Chem Phys Lett 325:589–598
26. Gudipati MS, Daverkausen J, Maus M, Hohlneicher G (1944) Higher electronically excited states of phenanthrene, carbazole and fluorene. Chem Phys 186:289–301
27. Benesi HA, Hildebrand JH (1949) J Am Chem Soc 71:2703–2707
28. Jing L, Qu Y, Wang B, Li S, Jiang B, Yang L, Fu W, Fu H, Sun J (2006) Review of photoluminescence performance of nano-sized semiconductor materials and its relationships with pho tocatalytic activity. Sol Energy Mater Sol Cells 90:1773–1787
29. Karunakaran C, SakthiRaadha S, Gomathisankar P, Vinayagamoorthy P (2013) Enhanced photocatalytic and bactericidal activities of carbon microsphere-assisted solvothermally synthesized cocoon-shaped Sn^{4+}-doped ZnO nanoparticles. Dalton Trans 42:13855–13865
30. Wang X, Zhang R, Wu C, Dai Y, Song M, Gutmann S, Gao F, Lv G, Li J, Li X, Guan Z, Fu D, Chen B (2007) The application of Fe_3O_4 nanoparticles in cancer research: a new strategy to inhibit drug resistance. J Biomed Mater Res Part B 80A:852–860
31. He WY, Li Y, Xue C, Hu ZD, Chen XG, Sheng FL (2005) Effect of Chinese medicine alpinetin on the structure of human serum albumin. Bioorg Med Chem 13:1837–1845
32. Kavarnos GJ, Turro NJ (1986) Photosensitization by reversible electron transfer: theories, experimental evidence, and examples. Chem Rev 86:401–449
33. Parret S, Savary FM, Fouassier JP, Ramamurthy P (1994) Spin-orbit-coupling-induced triplet formation of triphenylpyrylium ion: a flash photolysis study. J Photochem Photobiol A 83:205–209
34. Kikuchi K, Niwa T, Takahashi Y, Ikeda H, Miyashi T (1993) Quenching mechanism in a highly exothermic region of the Rehm-Weller relationship for electron-transfer fluorescence quenching. J Phys Chem 97:5070–5073
35. Thanikachalam V, Arunpandiyan A, Jayabharathi J, Ramanathan P (2014) Photophysical properties of the intramolecular excited charge–transfer states of π-expanded styryl phenanthrimidazoles – Effect of solvent polarity. RSC Adv 4:6790–6806
36. Xu S, Shen J, Chen S, Zhang M, Shen T (2002) Active oxygen species (1O2, O2·−) generation in the system of TiO2 colloid sensitized by hypocrellin B. J Photochem Photobiol A Chem 67:64–70
37. Sudeep PK, Takechi K, Kamat PV (2007) Harvesting photons in the infrared. Electron injection from excited tricarbocyanine dye (IR 125) into TiO_2 and Ag@TiO_2 core-shell nanoparticles. J Phys Chem C 111:488–494